



Impacts of cloudiness on near surface radiation and temperature in Nigeria, West Africa

Olaniran J. Matthew¹ · Muritala A. Ayoola² · Emmanuel O. Ogolo³ · Lukman A. Sunmonu²Received: 31 March 2020 / Accepted: 25 November 2020 / Published online: 1 December 2020
© Springer Nature Switzerland AG 2020

Abstract

This study investigates impacts of cloudiness on surface radiation budget and temperature from 1983 to 2018 in Nigeria, West Africa. The National Aeronautics and Space Administration meteorological datasets were used to achieve this objective. Net radiation (R) increased latitudinally from the coast to the inland areas. The least value of R was obtained in wet season which coincided with the period when cloud cover was at its optimal. We obtained significant decreasing trends (-0.110 to $-0.536 \text{ Wm}^{-2} \text{ year}^{-1}$) in R but significant increasing trends in cloud cover in most parts of the region. Under clear-sky conditions, however, significant increasing trends (0.256 – $0.807 \text{ Wm}^{-2} \text{ year}^{-1}$) in R were obtained. Annual mean temperature showed significant upward trends under all-sky (0.009 – $0.059 \text{ °C year}^{-1}$) and clear-sky (0.019 – $0.072 \text{ °C year}^{-1}$) conditions. Furthermore, significant negative correlations ($-0.70 \leq r \leq -0.95$) were obtained between monthly values of cloud cover and R over the country. However, r values for cloud cover and temperature were positive over Sahel ($r \sim 0.65$) but negative over Guinea ($r \sim 0.45$); both significant at $p < 0.05$. Changes in R were accounted for by 21 to 26% variations in cloud cover, while fluctuation in temperature was explained by about 14% variation in cloud cover over Sahel region at $p < 0.05$. Our results revealed that the surface radiation budget was significantly perturbed by variations in cloudiness which resulted in net cloud-radiative cooling (-30 Wm^{-2}) over Guinea but warming over Savannah (25 Wm^{-2}) and Sahel (50 Wm^{-2}) zones.

Keywords Cloudiness · Surface radiation budget · Radiative impacts · Temperature · Nigeria

1 Introduction

The interaction of solar radiation components with the earth's atmosphere maintains the energy balance and determines the temperature of the earth's surface [1, 2]. Thus, observations of the modulations of the shortwave (SW) and longwave (LW) by cloud-radiative forcing could provide useful insights into the cloud-climate interaction [3, 4].

Fraction of the incoming solar energy reflected by Earth back into atmosphere is called Earth's planetary (surface) albedo. It is a fundamental component of the processes

that govern the magnitude, distribution and variability of Earth's climate and climate change [5, 6]. Surface albedo is highly variable, depending on many factors, such as land-cover types, snow/ice cover, surface roughness or textural characteristics, mineral composition soil moisture content and human activities, such as deforestation, agriculture, irrigation, pollution and urbanization [7–12].

A linear relationship between the moisture content and surface albedo has been widely documented [13, 14]. In agreement with this assertion, Audu et al. [15] reported higher surface albedo (~ 0.6) in wet season than (~ 0.4) in dry season over Sahel region in northern Nigeria. They

✉ Olaniran J. Matthew, abefematt@yahoo.com | ¹Institute of Ecology and Environmental Studies, Obafemi Awolowo University, Ile-Ife, Nigeria. ²Department of Physics and Engineering Physics, Obafemi Awolowo University, Ile-Ife, Nigeria. ³Department of Physics, Federal University of Technology, Akure, Nigeria.



attributed higher albedo and lower incoming solar radiation obtained in wet season to the rain-bearing clouds which pervaded the sky in the rainy season compared to the dry season. It has also been reported that natural phenomena such as wild fire could alter surface albedo [12, 16–18].

The spatial and temporal variation of the surface net (all-wave) radiation, which is the sum of SW and LW net radiation, is responsible for the re-distribution of the available energy. For example, net radiation controls the inputs of latent and sensible heat fluxes into the atmosphere, and the oceanic heating over the ocean [12]. Radiative forcing is an externally imposed change in the radiative energy budget of the Earth's climate system [19]. The energy budget is characterized by an approximate balance between SW absorption and LW emission by the climate system [20–22]. Change in radiative forcing, which can affect either the SW or LW components of the radiative budget, can be caused by a number of factors such as variations in solar insolation, alteration in surface boundary conditions related to land use change and desertification, or natural and anthropogenic perturbations to the radiatively active species in the atmosphere known as greenhouse gases e.g. CO₂, CH₄, N₂O and the halocarbons [21, 23].

Furthermore, clouds and aerosols can exert a strong influence on regional radiative balance by reflecting SW radiation back to space, emitting LW radiation to the surface and absorbing LW radiation emitted by the warmer earth; thereby providing one of the strongest feedback pathways in the climate system [4, 24–28]. Thus, changes in aerosol loading and cloud cover as well as cloud properties could cause a significant reduction in surface solar radiation [29]. In addition, because clouds interact so strongly with both SW and LW radiation, small changes in cloudiness could have a large effect on the climate system [30, 31]. Atmospheric cloud-radiative effects (CRE) describe the change in radiative heating within the atmosphere owing to clouds. The literature revealed that CRE increases with cloud cover and decreases with the solar zenith angles [32]. It has also been reported that the effects of clouds on the radiation balance at the top-of-the-atmosphere (TOA) and within the troposphere are quite different from their effect at the Earth's surface [3, 33]. Clouds, on average, is found to cool the surface by reflecting SW radiation and warm it by increasing the downward flux of LW radiation [26]. Thus, the effect of clouds on the atmospheric energy budget, however, is found to be less straightforward [33]. Also, clouds could either warm or cool the atmosphere, depending on their vertical structure. For example, Slingo and Slingo [34] reported that low clouds can cool the atmosphere by increasing the downward emission of LW radiation, while high clouds warm it by decreasing the

upward emission of LW radiation. Within deep convection in the tropics, where high clouds dominate, cloud-radiation interactions warm the upper troposphere because absorption of LW and SW radiation is much larger than the cloudy emission of LW radiation [33, 35]. Similarly, isolated low clouds were found to cause net radiative cooling of the atmosphere, which reduces the warming from other cloud types by approximately 10% [36]. The combination of these effects increases the cloud-radiative effect at the TOA. It has also been shown that perturbations to the atmospheric radiation budget, that are induced by cloud changes in response to climate forcing, dictate the eventual response of the global-mean hydrological cycle to climate forcing [24]. Hence, little changes in the cloud-radiative forcing fields can play a significant role as a climate feedback mechanism [3, 33].

Several studies have investigated variations and implications of surface radiation balance on the climate of West Africa [14, 25, 37–42]. The literature revealed significant variations in seasonal patterns of net radiation over the humid tropical rainforest (*i.e.* Guinea zone) [9], and the Sahelian region of West Africa [41]. It has also been documented that cloud processes, level and types modulate LW and SW radiation components, which affect surface temperature and water cycle in the region [25]. During the wet season (July and August), the heavy cloud blocks the direct component of the solar irradiance resulting to the observed minimum value of daily energy over West Africa [41, 42]. It has been shown that dust particles have a complex impact on the radiative transfer process because of their ability to interact both in shortwave and longwave radiation [29]. As such, due to the fact that West Africa is notably subject to large smoke and mineral dust loads, the regional radiative budget is found to be significantly impacted [39, 43]. Annual cycle of radiation is also reported to have a substantial influence on the seasonal variation of the monsoon system over West Africa [44]. However, some previous studies over West Africa used radiative models to estimate radiation components, while a few others used ground measurements for just a few periods of time e.g. 1 to 24 months [37–39]. This was so because long-term data (for more than 2 years) on net radiation are still scarce for most parts of West Africa [37] due to high cost of maintenance of net radiation measurements on a continuous long-time basis [9, 45]. Thus, availability of satellite-derived radiation data such as those provided by the National Aeronautics and Space Administration (NASA) promises to complement the paucity of these measurements, even though such data do not have the spatial or temporal resolution that in situ net radiation sensors provide. Some of these available studies revealed that cloud formation is a major source of uncertainty for future climate projections through a diversity of feedbacks

between clouds and radiative processes in the region. In addition, dust particles during the dry Harmattan season, particularly in the West African Sahel, have been shown to have a complex impact on the radiative transfer process because of their ability to interact both in SW and LW radiation [25]. However, long-term variation in surface radiation balance and its impacts on cloudiness in different parts of West Africa is still not yet fully understood. Therefore, the present study investigates annual and seasonal variations in cloud cover from 1983 to 2018 and their impacts on the surface radiation budget and temperature over different climatic zones of Nigeria.

2 Materials and methods

2.1 Study area

Nigeria (Fig. 1) has a unique tropical climate with two prominent seasons dominated by the West African monsoon, WAM [46–48]. WAM flow produces a wet season of several months of rainfall and a dry season during which

the low-level flow transports hot and dry air from the Sahara Desert into the northern Sahel [40]. The most clearly marked spatial differences in the regional climate are found between the highly humid and relatively colder zone in the south and a semi-arid region in the interior north [49]. The wet season is longer in the south (April–October) than the north (May/June–September) while total annual rainfall are within the range of 1500–2000 mm/year and 450–600 mm/year in the south and north, respectively [50, 51]. Daily temperature in the south and northern parts of the country ranges from 23 to 32 °C and 18 to 38 °C, respectively [52]. The topography and vegetation zones are shown in Fig. 1. The topography ranges from lowland (20–100 m) along the Atlantic coastline areas in the south to high plateau in the central north (700–800 m) and mountains (800–1500 m) along the eastern border (Fig. 1b). The southern coastline areas are covered with mangrove forest and fresh water swamp (Fig. 1c). It is followed by rainforest in the southwestern zone, tall and short grass savannah in the central and parts of the northern zones as well as marginal savannah in the north-eastern border.

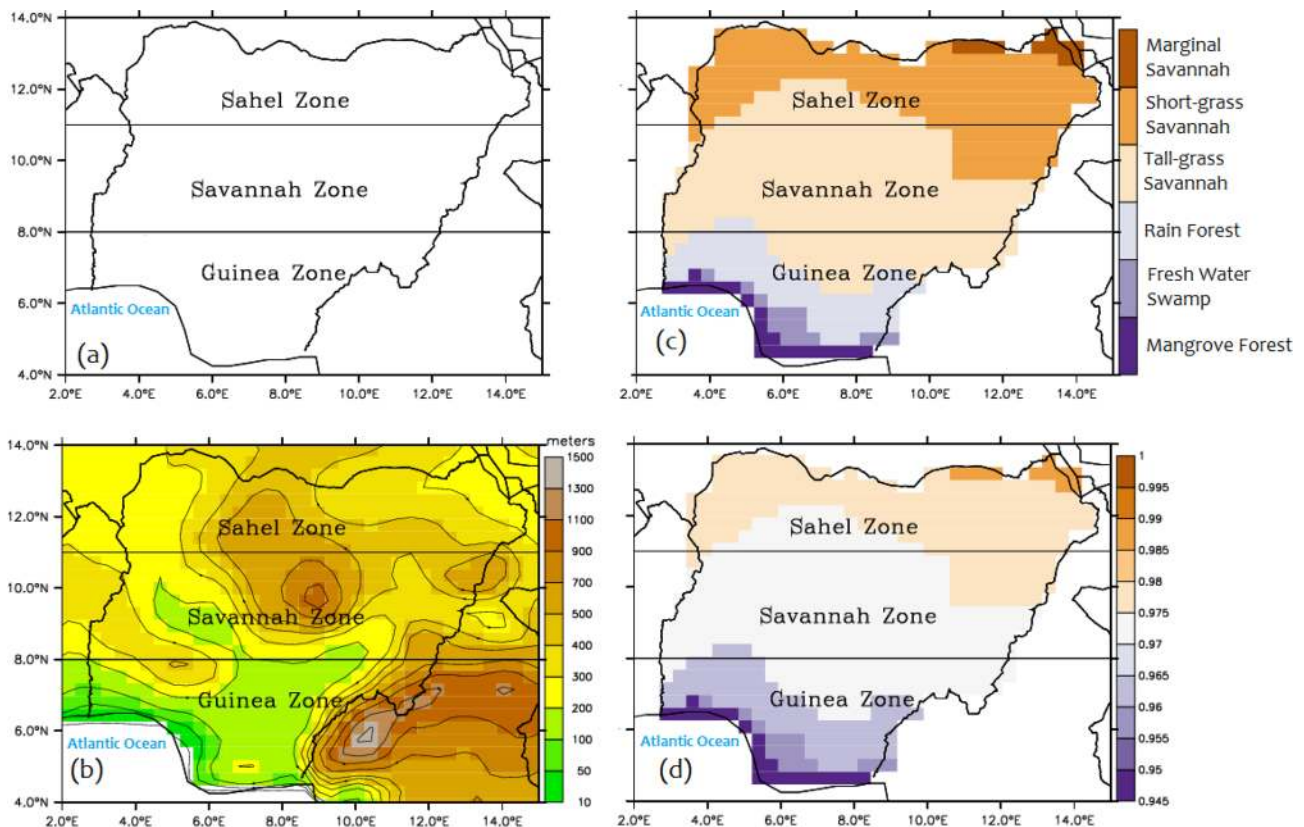


Fig. 1 Sketch map of Nigeria showing **a** the climatic regions designated as Guinea, Savannah and Sahel zones; **b** topography; **c** vegetation zones; and **d** surface emissivity

2.2 Data source

Essentially, we analyzed monthly climatology datasets of surface radiation components, near and skin surface temperatures as well as cloud cover of the National Aeronautics and Space Administration’s (NASA) Modern-Era Retrospective Analysis for Research and Applications (MERRA) for 1983–2018 period over Nigeria, West Africa (Fig. 1a). The data were obtained from the archive of the Prediction of Worldwide Energy Resource (POWER) project supported by the National Aeronautics and Space Administration (NASA) and Langley Research Center, LaRC (<https://power.larc.nasa.gov/>). They are improved global meteorological datasets generated with version 5.12.4 of the Goddard Earth Observing System (GEOS) atmospheric model and data assimilation system (DAS) with spatial resolution of 0.5 degree longitude and 0.5 degree latitude [53, 54]. The performance of NASA-MERRA data product for global solar radiation had been previously evaluated and validated over Nigeria, West Africa [55, 56] and other regions around the world e.g. China [57], Pakistan [58], Brazil [59] and wider areas [60]. These studies show that the datasets exhibit tolerable discrepancies compared with ground observations (and other global reanalyses) and provide scientific reference for rational use of NASA datasets in the selected regions. Consequently, the products have been widely used for climate impacts studies over different parts of the world including Nigeria, West Africa [61, 62].

2.3 Methods and data processing

Data analyses were carried out over the entire Nigerian domain (4°N–14°N; 2°E–15°E) with a special focus on three designated climatic zones (Fig. 1a) using a widely used climate classification method over West Africa based on similarities in land-use/land-cover, climate and ecosystems [48, 52]. These zones are: (1) Guinea (between latitude 4°N and 8°N); (2) Savannah, (8°N and 11°N and; (3) Sahel (11°N and 14°N). This classification enables us to effectively assess the contributions of cloud cover on the radiation budget over different parts of the country. The relevant NASA’s MERRA datasets obtained, as provided by POWER, consist of, cloud cover fraction, surface albedo, near surface temperature (at 2 m), skin surface temperature, all-sky downwelling (incoming) shortwave (SW) radiation, $R_{S\downarrow}$ and longwave (LW) radiation, $R_{L\downarrow}$ as well as clear-sky downwelling SW. Following the convection of signs, downwelling and upwelling radiations at the earth surface are positive and negative, respectively.

The upwelling SW radiation, $R_{S\uparrow}$, under all-sky and clear-sky conditions was estimated as the fraction of the corresponding $R_{S\downarrow}$ that is reflected by the surface, i.e.,

$$R_{S\uparrow} = \alpha R_{S\downarrow} \tag{1}$$

where α is the surface albedo.

The net SW radiation, R_S , under all-sky and clear-sky conditions were then estimated as:

$$R_S = R_{S\downarrow} - R_{S\uparrow} \tag{2}$$

The upwelling LW radiation $R_{L\uparrow}$ under all-sky conditions and both $R_{L\downarrow}$ and $R_{L\uparrow}$ under clear-sky were estimated using the Stefan–Boltzmann equation (Eq. 3) and the parameterization scheme for atmospheric emissivity (Eq. 4) proposed by Staley and Jurica [63] as widely used in the literature [64–66]. Specifically, LW radiation $R_{L\uparrow}$ under all-sky and clear-sky conditions was obtained as:

$$R_{L\uparrow} = \sigma \epsilon_s T_s^4 \tag{3}$$

where ϵ_s of the emissivity of the surface, sigma is the Stefan–Boltzmann constant ($5.6705 \times 10^{-8} \text{ W m}^{-2} \text{ K}^{-4}$) and T_s the skin surface temperature in kelvin under all-sky or clear-sky conditions. The country’s vegetation cover classification in Fig. 1c (adapted from Abiodun et al. [52]) was used to derive spatial distribution of surface emissivity (Fig. 1d) using the values previously obtained with remote-sensing technology over the region [67] and similar vegetation types elsewhere [68, 69].

For $R_{L\downarrow}$ under clear-sky conditions, however, we used air temperature, T_a in Eq. (3) with the following expression for atmospheric emissivity, ϵ_a [1, 64]:

$$\epsilon_a = 0.67 P_w^{0.08} \tag{4}$$

where P_w is the partial water pressure/actual vapor pressure in hectopascal expressed as a function of relative humidity, RH (%) and temperature [70, 71]:

$$P_w = 6.1078 \exp \left(\frac{17.27 T_a}{273.3 + T_a} \right) \times \text{RH}/100 \tag{5}$$

Then, the net LW radiation, R_L and net (all-wave) radiation, R , are given in Eqs. (6) and (7):

$$R_L = R_{L\downarrow} - R_{L\uparrow} \tag{6}$$

$$R = R_S - R_L \tag{7}$$

Cloud-radiative effects for shortwave (CRE_{SW}) and longwave (CRE_{LW}) were estimated as [3, 26, 30]:

$$\text{CRE}_{\text{SW}} = (R_{S\uparrow} - R_{S\downarrow})_{\text{clear-sky}} - [R_{S\uparrow} - R_{S\downarrow}]_{\text{all-sky}} \tag{8a}$$

$$\text{CRE}_{\text{LW}} = (R_{L\uparrow} - R_{L\downarrow})_{\text{clear-sky}} - [R_{L\uparrow} - R_{L\downarrow}]_{\text{all-sky}} \tag{8b}$$

The values of CRE_{SW} and CRE_{LW} provide measure of the impacts of clouds on SW and LW radiation, respectively—where positive CRE_{SW} or CRE_{LW} means heating effect and their negative values indicate cooling effect.

Then, the net radiative effects CRE was computed as:

$$CRE = CRE_{SW} + CRE_{LW} \quad (9)$$

Analysis of inter-annual and seasonal variations in surface radiation budget, temperature and cloud cover was obtained, and the results were presented and discussed. For all the years (1983–2018), the standardized anomaly, φ , was calculated as:

$$\varphi = \frac{x - \bar{x}}{\sigma} \quad (10)$$

where x is the actual value of each parameters (radiation components, temperature and cloud cover), \bar{x} is their long-term means and σ the standard deviations.

We adopted a least-square-fit and Mann–Kendall, MK test [72, 73] to investigate the magnitudes and significance of the annual trends of all the parameters at 99% (0.1), 95% (0.05) and 90% (0.01) confidence levels. The MK statistics, as fully described in the literature [51, 74, 75], is a nonparametric trend test which is often used to test for trends in climatological-data time series. In addition, correlations between all monthly mean values (1983–2018) of cloud cover and radiation components as well as temperature were computed, while a linear regression analysis was performed to determine the contributions of cloudiness (independent variable) to surface radiation budget and temperature.

3 Results and discussion

3.1 Annual mean variations in surface radiation budget and temperature

Figure 2 depicts the long-term annual mean (1983–2018) spatial variations in both upwelling and downwelling radiation components under all-sky condition over Nigeria. By sign conventions, positive and negative signs denote downwelling and upwelling radiation components, respectively. Downwelling SW ($R_{S\downarrow}$) and LW ($R_{L\downarrow}$) radiation were about 200 and 410 Wm^{-2} over the Guinea zone, respectively (Fig. 2a, b). Their estimates over Sahel were 270 Wm^{-2} ($R_{S\downarrow}$) and 375 Wm^{-2} ($R_{L\downarrow}$). Results, thus, revealed that $R_{S\downarrow}$ increased inland from the coast, while $R_{L\downarrow}$ decreased inland. This could be explained by spatial distribution of cloud cover which decreases inland from the coast. Our results further confirm previous findings that $R_{S\downarrow}$ over West Africa increases latitudinally from the coast

[55, 76]. The upwelling SW ($R_{S\uparrow}$) and LW ($R_{L\uparrow}$) radiation were -35 and $-440 Wm^{-2}$ over Guinea, respectively, while $R_{S\uparrow} \approx -90 Wm^{-2}$ and $R_{L\uparrow} \approx -460 Wm^{-2}$ over Sahel (Fig. 2c, d). Net SW (R_S) and LW (R_L) radiation were about 150 and $-20 Wm^{-2}$ over Guinea, respectively (Fig. 2e, f). However, the values of R_S ($\approx 180 Wm^{-2}$) and R_L ($\approx -170 Wm^{-2}$) were higher in both Sahel and Savannah than in the Guinea (130 and 40 Wm^{-2} , respectively). The values obtained were within the range of values previously reported in literature [9, 77]. Furthermore, annual mean variations in R_S and R_L radiation components under clear-sky are shown in Fig. 3. As expected, R_S radiation components under clear-sky were generally higher in magnitudes than their values under all-sky condition while those of R_L components were reverse [78]. Over the country, $R_{S\downarrow}$ ranged between 255 Wm^{-2} (in Guinea) and 290 Wm^{-2} (Sahel) while $R_{S\uparrow}$ ranged between $-40 Wm^{-2}$ (Guinea) and $-100 Wm^{-2}$ (Sahel) (Fig. 3a, b). Under clear-sky condition, $R_{L\downarrow}$ were 395 Wm^{-2} over Guinea and 365 Wm^{-2} over Sahel while $R_{L\uparrow}$ were -445 and $-470 Wm^{-2}$ over Guinea and Sahel, respectively (Fig. 3c, d).

The net (all-wave) radiation, R , were about 180 Wm^{-2} over Guinea, 240 Wm^{-2} over Savannah and 280 Wm^{-2} over Sahel (Fig. 4a). This demonstrated that R generally increases with increasing latitude. Cloud cover fraction were about 80% over Guinea, 50% over Savannah and 45% over Sahel (Fig. 4b). Surface albedo and temperature were 0.20:25.0 °C over Guinea and 0.30:28.0 °C over Sahel, respectively (Fig. 4c, d). Observed spatial distribution of R over the country suggested higher surface heating in the semi-arid regions (Savannah and Sahel) than in the Guinea. Similar spatial variations in R have been reported in the analysis of net radiation data over West Africa by Ojo [79] and Hayward and Oguntoyinbo [80]. These results supported the fact that R is highly dependent on geographical location, time of the day, season, cloud cover, surface temperature, and type and conditions of the surface as indicated by albedo and emissivity [81, 82]. Increased $R_{S\downarrow}$ and R with increasing latitude have been attributed to the observed spatial pattern of cloud cover [76]. Different levels and categories of cloud have been found to reduce $R_{S\downarrow}$ significantly in the tropics [25]. Thus, future changes in cloudiness and atmospheric aerosols could have significant impacts on surface temperature and the rate of evapotranspiration, with important consequences on atmosphere–surface interactions and the regional hydrological cycle as speculated by Bounioul et al. [25]. In addition, we found that the potential of the ground surface to reflect $R_{S\downarrow}$ is higher in the Sahel region as remonstrated by the spatial distribution of surface albedo in Fig. 4c. This supports higher $R_{S\downarrow}$ recorded in Sahel compared to the Guinea zone in the south. Variations in cloudiness have been found to significantly modulate the

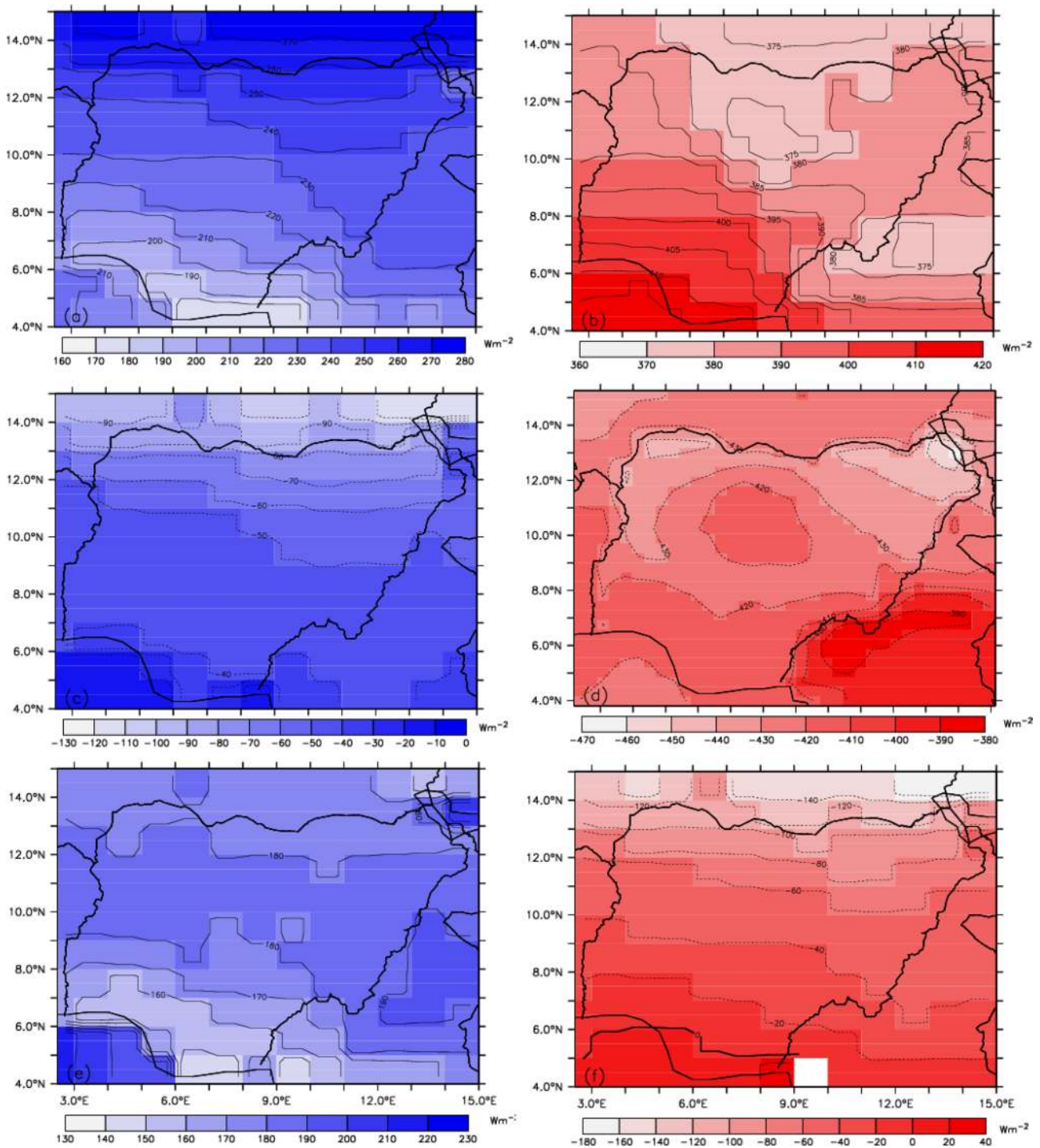


Fig. 2 Annual means of all-sky over Nigeria (1983–2018): **a** downwelling shortwave radiation, $R_{S\downarrow}$ **b** downwelling LW radiation, $R_{L\downarrow}$ **c** upwelling SW radiation, $R_{S\uparrow}$ **d** upwelling LW, $R_{L\uparrow}$ **e** net SW radiation,

R_S and **f** net LW radiation, R_L . By convention, positive and negative signs denote downwelling and upwelling radiation components, respectively

atmospheric emissivity, temperature distribution and the general circulation of the atmosphere which are the most important regulators of the Earth’s climate [14, 83]. Thus, potential future variations in cloud cover and radiation

budget over the country could have significant impact on the regional climate. Moreover, the observed pattern of cloud cover produced lower $R_{S\downarrow}$ ($\sim 200 \text{ Wm}^{-2}$) in Guinea than ($\sim 265 \text{ Wm}^{-2}$) Sahel but higher $R_{L\downarrow}$ ($\sim 400 \text{ Wm}^{-2}$) over

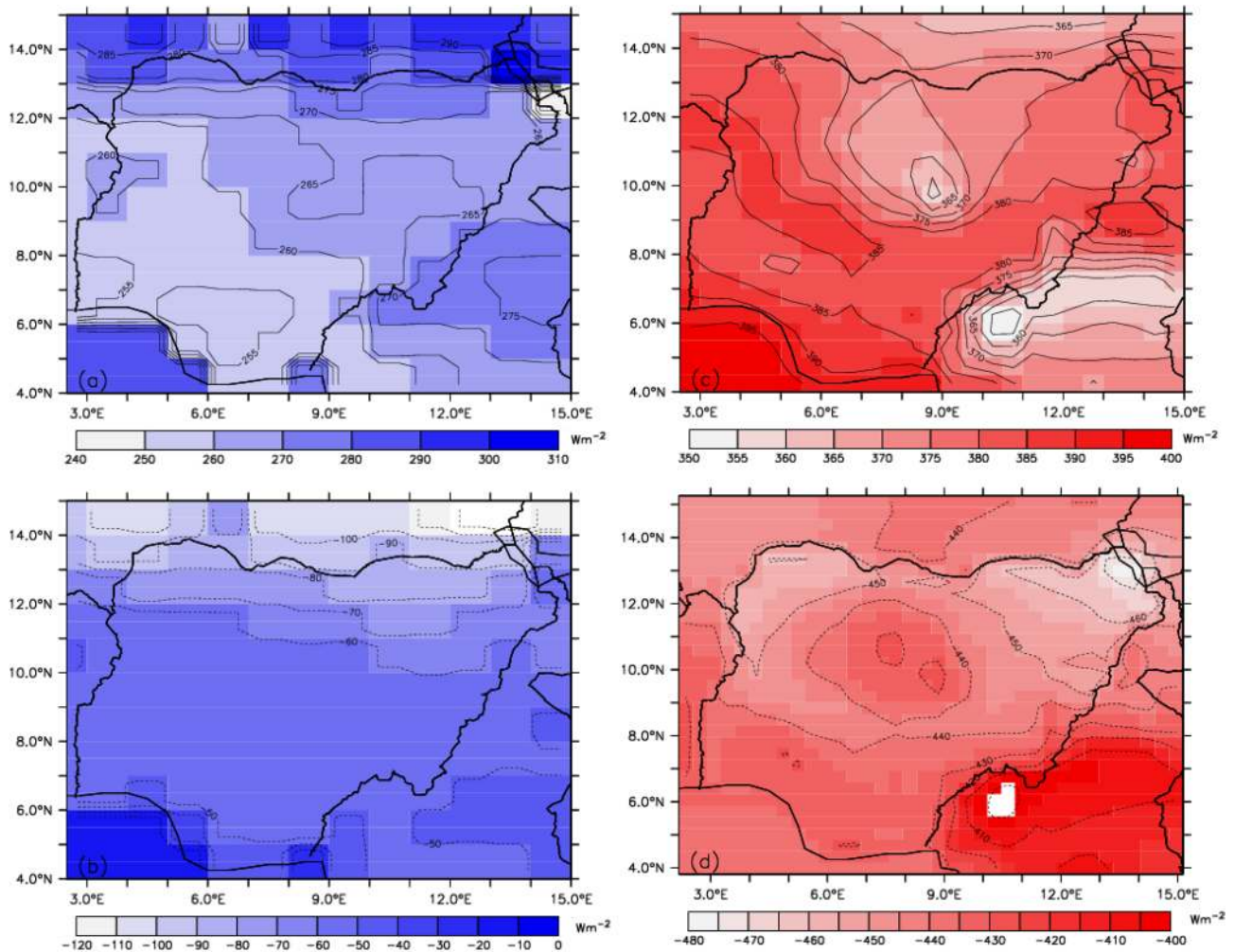


Fig. 3 Annual means of clear-sky over Nigeria (1983–2018): **a** downwelling SW radiation, $R_{S\downarrow}$ **b** upwelling SW radiation, $R_{S\uparrow}$ **c** downwelling LW radiation, $R_{L\downarrow}$ and **d** upwelling LW radiation, $R_{L\uparrow}$. By

convection, positive and negative signs denote downwelling and upwelling radiation components, respectively

Guinea than ($\sim 380 \text{ Wm}^{-2}$) Sahel. This is a signal that higher cloud cover fraction enhances $R_{L\downarrow}$ [30]. Higher temperature obtained in Sahel could be attributed to higher R recorded in the zone. However, surface temperature in Guinea is moderated by cool monsoon air from the Atlantic Ocean (known as the West African Monsoon, WAM) and the presence of thick vegetation in the region [52, 55, 84] which significantly reduces warming effects of enhanced $R_{L\downarrow}$ over the region.

3.2 Inter-annual variations and trends

Figures 5 and 6 represent the inter-annual variations (in terms of standardized anomaly) and the trend lines of the four radiation components under all-sky and clear-sky conditions, respectively. Results suggested high spatial and temporal inter-annual variability in radiation components

over the country during the study period (1983–2018). For example, both $R_{S\downarrow}$ and $R_{S\uparrow}$ had more of negative anomalies, while positive anomalies were predominant for $R_{L\downarrow}$ and $R_{L\uparrow}$ under all-sky condition in all the three climatic zones (Fig. 5). However, all the four radiation components under clear-sky showed positive anomalies (Fig. 6). The anomalies obtained for all the radiation components under both sky conditions ranged between -2.2 and 2.2 .

Summary of results of all the trend analysis is presented in Table 1. The positive values of MK statistics indicate upward trend line, while the negative values show the downward trend at $p=0.01$, 0.05 , and 0.10 confidence levels. Results revealed decreasing trends in $R_{S\downarrow}$ (Guinea = $-0.268 \text{ Wm}^{-2} \text{ year}^{-1}$, Savannah = $-0.207 \text{ Wm}^{-2} \text{ year}^{-1}$ and Sahel = $-0.116 \text{ Wm}^{-2} \text{ year}^{-1}$) and $R_{S\uparrow}$ (Guinea = $-0.218 \text{ Wm}^{-2} \text{ year}^{-1}$, Savannah = $-0.165 \text{ Wm}^{-2} \text{ year}^{-1}$ and Sahel = $-0.084 \text{ Wm}^{-2} \text{ year}^{-1}$)

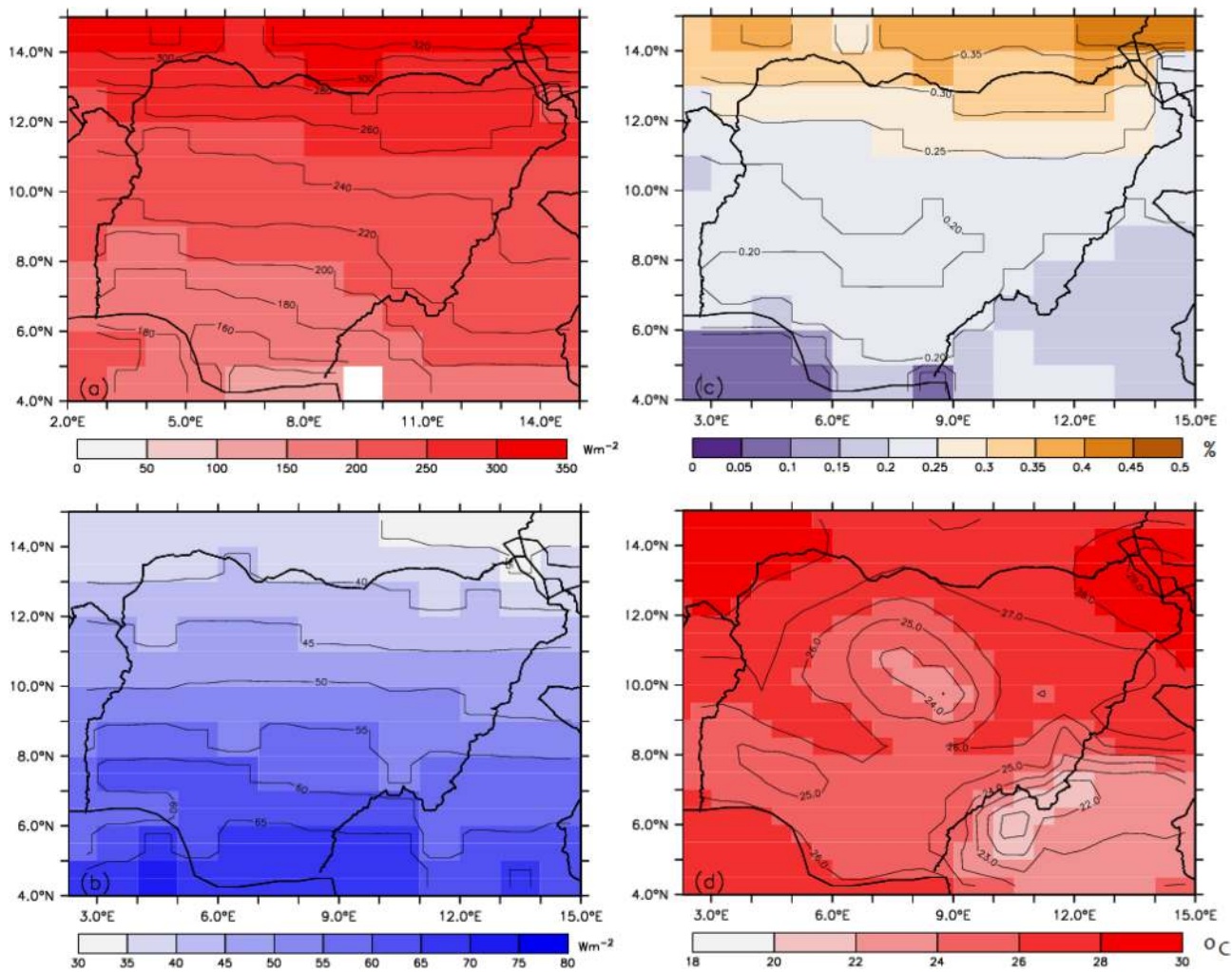


Fig. 4 Spatial distribution of annual means of **a** net (all-wave) radiation, R (Wm^{-2}), **b** cloud cover fraction (%), **c** surface albedo (dimensionless), and **d** near surface temperature ($^{\circ}\text{C}$) over Nigeria (1983–2018)

under all-sky conditions (Table 1). These trends in SW radiation components were found to be significant except in the Sahel zone. Results further indicated that there have been statistically significant increases in $R_{L\downarrow}$ (Guinea = 0.585, Savannah = 0.257 and Sahel = 0.215) and $R_{L\uparrow}$ (Savannah = 0.422 and Sahel = 0.124). However, the upward trend of $R_{L\uparrow}$ (0.018) over Guinea was found to be insignificant. Consequently, decreasing trends (-0.110 to $-0.536 \text{ Wm}^{-2} \text{ year}^{-1}$) in R were obtained under all-sky in all the zones. Cloud cover showed significant increasing trends over Guinea ($0.473\% \text{ year}^{-1}$) and Sahel ($0.081\% \text{ year}^{-1}$), but decreasing and insignificant trend was obtained over Savannah ($-0.026\% \text{ year}^{-1}$). On the other hand, all the four radiation components showed increasing trends (0.114 – $0.559 \text{ Wm}^{-2} \text{ year}^{-1}$) under clear-sky conditions in all the zones (Table 1). These changes were found to be significant except the trend of $R_{L\uparrow}$ ($0.017 \text{ Wm}^{-2} \text{ year}^{-1}$) obtained over the Guinea zone. Significant upward

trends in R (0.256 – $0.807 \text{ Wm}^{-2} \text{ year}^{-1}$) were estimated over all zones, contrary to downward trends obtained under all-sky condition. Results showed significant upward trends in temperature under all-sky (0.009 – $0.059 \text{ }^{\circ}\text{C} \text{ year}^{-1}$) and clear-sky (0.019 – $0.072 \text{ }^{\circ}\text{C} \text{ year}^{-1}$) conditions over the entire region. In brief, results of the 36-year trend analysis suggested warmer climate over the entire country, in agreement with the previous studies [48, 52] and demonstrated that the surface radiation and temperature had been significantly perturbed due to changes in cloud-radiative forcing as speculated in the literature [e.g. 3, 21, 23–36].

3.3 Seasonal mean variations

Variations in seasonal or annual cycle of surface radiation balance in different designated climatic zones of Nigeria are illustrated in Fig. 7. The lowest (157 Wm^{-2} (Guinea), 181 Wm^{-2} (Savannah) and 220 Wm^{-2} (Sahel))

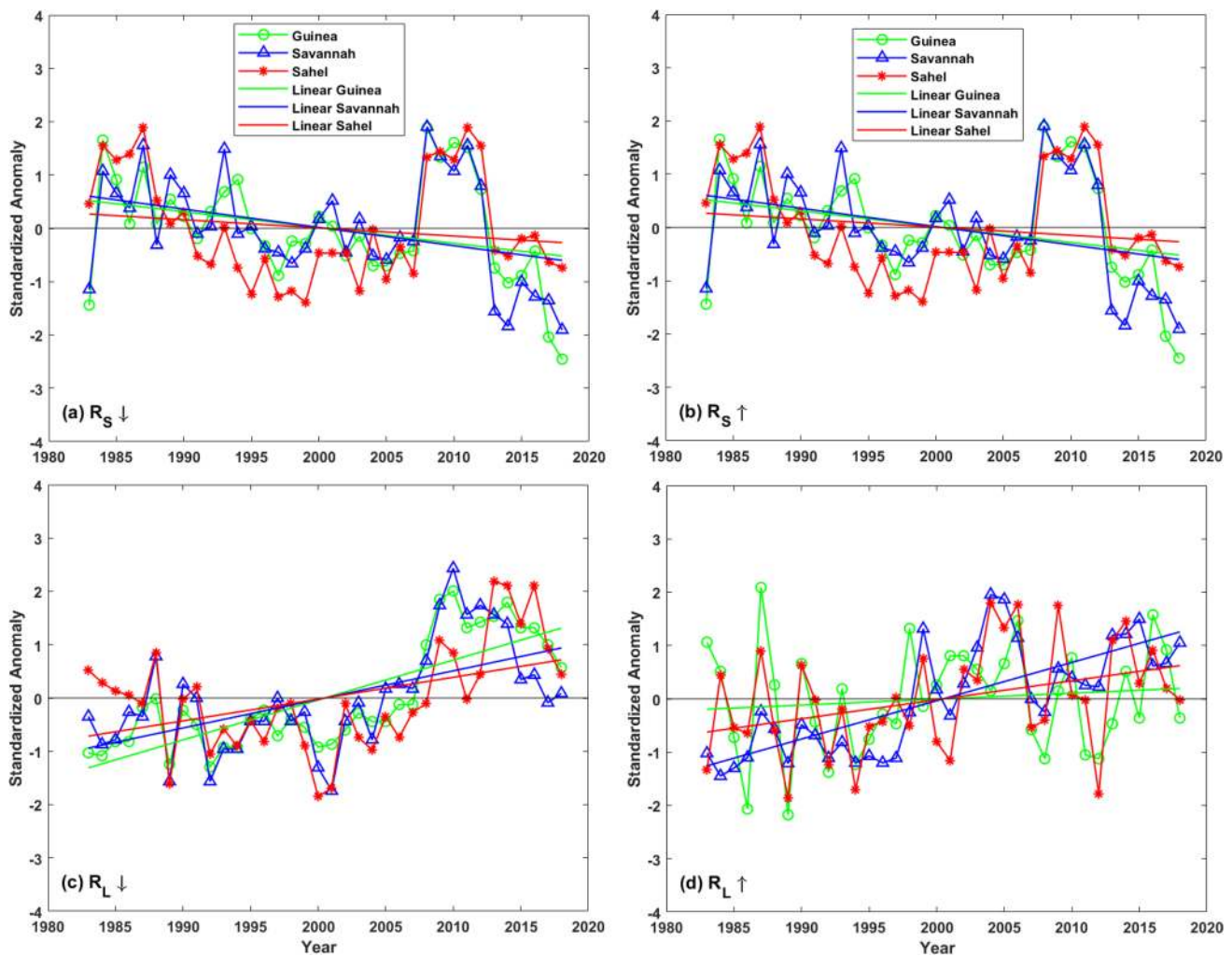


Fig. 5 Inter-annual variability (standardized anomaly) in radiation components under all-sky conditions over Guinea, Savannah, and Sahel regions of Nigeria (1983–2018): **a** downwelling SW, $R_{S\downarrow}$ **b** upwelling SW, $R_{S\uparrow}$ **c** downwelling LW, $R_{L\downarrow}$ and **d** upwelling LW radiations, $R_{L\uparrow}$

and the peak (231 Wm^{-2} (Guinea), 260 Wm^{-2} (Savannah) and 282 Wm^{-2} (Sahel)) of $R_{S\downarrow}$ occurred in July/August and February/April over the country, respectively (Fig. 7a). $R_{S\uparrow}$ was generally lower than $R_{S\downarrow}$ and recorded its lowest (-60 Wm^{-2} (Guinea), -70 Wm^{-2} (Savannah) and -86 Wm^{-2} (Sahel)) and the highest (-70 Wm^{-2} (Guinea), -83 Wm^{-2} (Savannah) and -115 Wm^{-2} (Sahel)) in August and March/April, respectively (Fig. 7c). In brief, the highest values of $R_{S\downarrow}$ and $R_{S\uparrow}$ were obtained in late dry season (February–March in Guinea; April–May in Savannah and Sahel) and the least in the wet season (July–August) over the country. Seasonal pattern of $R_{L\downarrow}$ was opposite to the R_S components with the peak in dry season and the lowest in the wet. This might not be unconnected with the cloud-radiative impact. Higher cloud cover during the wet season increases the atmospheric emissivity and thus enhances $R_{L\downarrow}$. Observed spatial pattern and magnitudes of $R_{L\downarrow}$ followed that of temperature (with the

highest over the north) as explained by the Stefan–Boltzmann Eq. (3).

Figure 8 shows the seasonal variations in net radiation (R), cloud cover, surface albedo and temperature. Results showed that R had the least values (100 , 121 and 171 Wm^{-2} over Guinea, Savannah and Sahel, respectively) in the peak of the wet season and the highest (245 Wm^{-2} (Guinea), 310 Wm^{-2} (Savannah and Sahel)) in dry season (Fig. 8a). The peak of cloud cover (79% (Guinea), 80% (Savannah, and 66% (Sahel)) occurred in wet season (August–September), while the least (38% (Guinea), 22% (Savannah, and 21% (Sahel)) were recorded in the dry period (January–March) (Fig. 8b). Seasonal variations in surface albedo were similar in Guinea and Savannah zones with the peak (0.22 (Guinea) and 0.28 (Savannah)) and the lowest values (0.17 (Guinea) and 0.18 (Savannah)) in wet and dry seasons, respectively. In contrast, the maximum (0.29) and the least (0.25) surface albedo were obtained in dry and

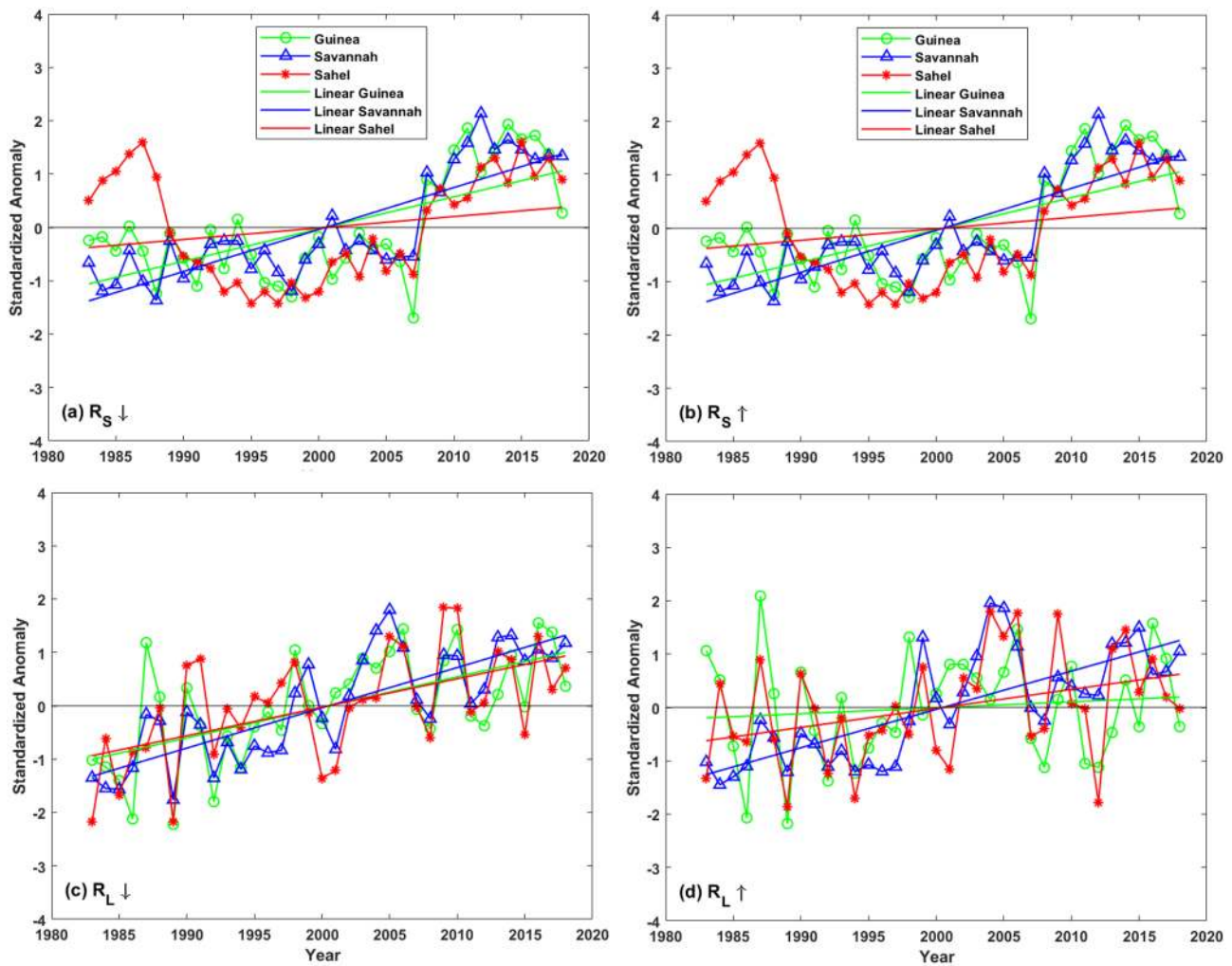


Fig. 6 Inter-annual variability (standardized anomaly) in radiation components under clear-sky conditions over Guinea, Savannah, and Sahel regions of Nigeria (1983–2018): **a** downwelling SW, $R_{S\downarrow}$ **b** upwelling SW, $R_{S\uparrow}$ **c** downwelling LW, $R_{L\downarrow}$ and **d** upwelling LW radiations, $R_{L\uparrow}$

wet seasons, respectively (Fig. 6c). Similarly, the highest (26.9 °C (Guinea), 28.3 °C (Savannah, and 31.2 °C (Sahel)) and the least (24.4 °C (Guinea), 23.4 °C (Savannah, and 22.1 °C (Sahel)) temperatures were recorded in dry and wet seasons. These are indications that the entire country is warmer in dry season than the wet. Results support the fact that cooling effect during the monsoon season is mainly due to the dominance of R_S in the net cloud-radiative forcing [25]. Higher cloudiness during the wet (monsoon) season could be attributed to lower R values recorded during this season [85]. In addition, the results in agreements with the literature [7, 13, 14, 86] suggested that higher albedo during the wet season was due to rise in soil moisture. Over Sahel, however, the least in surface albedo occurred in wet season (i.e., September) and highest in the dry (March). This could be as a result of combined effects of surface cover type, color, surface roughness or textural characteristics, mineral composition and

organic matter more than the soil moisture content in the region. However, this is at variance with the findings of Audu et al. [15] where albedo estimate over a location in the Sahel region was reported to be higher in wet season (September) than dry season. The reasons for this disparity could not be ascertained. However, the reason could be attributed to the latent error in (NASA's MERRA) satellite surface measurements due to interference of high atmospheric aerosol and Harmattan dust in West African Sahel during the dry season.

3.4 Relationship between cloudiness, surface radiation budget and temperature

The relationship between cloud cover and radiation budget components as well as temperature is shown in Fig. 9. The results indicated significant negative correlations ($r \sim -0.80$ at $p \leq 0.05$) between cloud cover and $R_{S\downarrow}$

Table 1 Trend analysis of the Mann–Kendall (MK) for annual radiation components and other meteorological indices in different designated climatic regions of Nigeria

Sky conditions	Indices	Zone		Savannah						Sahel						
		Guinea		Savannah			Sahel			Savannah			Sahel			
		S	Z	Trend	Sig.	m	S	Z	Trend	Sig.	m	S	Z	Trend	Sig.	m
All-sky	$R_s \downarrow$	-188.0	-2.547	↓	***	-0.268	-178.0	-2.411	↓	**	-0.207	-71.0	-0.954	↓	-	-0.116
	$R_s \uparrow$	-188.0	-2.547	↓	***	-0.218	-178.0	-2.411	↓	**	-0.165	-71.0	-0.954	↓	-	-0.084
	$R_L \downarrow$	336.0	4.563	↑	***	0.585	247.0	3.351	↑	***	0.257	138.0	1.866	↑	*	0.215
	$R_L \uparrow$	50.0	0.667	↑	-	0.018	348.0	4.727	↑	***	0.422	166.0	2.247	↑	**	0.124
	R	-80.0	-1.076	↓	-	-0.082	-216.0	-2.930	↓	***	-0.536	-42.0	-0.559	↓	-	-0.110
	CLD	130.0	1.757	↓	*	0.473	-88.00	-1.185	↓	-	-0.026	114.00	1.539	↑	*	0.081
Clear-sky	TMP	147.0	1.989	↑	**	0.009	367.0	4.985	↑	***	0.059	193.0	2.615	↑	***	0.022
	$R_s \downarrow$	226.0	3.065	↑	***	0.382	357.0	4.849	↑	***	0.559	124.0	1.675	↑	*	0.163
	$R_s \uparrow$	226.0	3.065	↑	***	0.312	357.0	4.849	↑	***	0.445	124.0	1.675	↑	*	0.118
	$R_L \downarrow$	266.0	3.610	↑	***	0.114	362.0	4.917	↑	***	0.257	248.0	3.364	↑	***	0.146
	$R_L \uparrow$	50.0	0.667	↑	-	0.017	348.0	4.727	↑	***	0.410	166.0	2.247	↑	**	0.121
	R	144.0	1.948	↑	**	0.256	248.0	3.364	↑	***	0.515	234.0	3.174	↑	***	0.807
All-sky	CLD	-	-	-	-	-	-	-	-	-	-	-	-	-	-	-
	TMP	50.0	0.667	↑	*	0.019	348.0	4.727	↑	***	0.072	166.0	2.247	↑	**	0.028

S = MK test statistic, Z = standardized MK score and m = slope of the trend line

↑ = increasing trend, ↓ = decreasing trend

$R_{s\downarrow}$ = downwelling SW, $R_{s\uparrow}$ = upwelling SW, $R_{L\downarrow}$ = downwelling LW, $R_{L\uparrow}$ = upwelling LW, R = net radiation, CLD = cloud cover, and TMP = temperature

Sig. = Significant status; * means significant at $p = 0.1$, ** means significant at $p = 0.05$ and *** means significant at $p = 0.01$

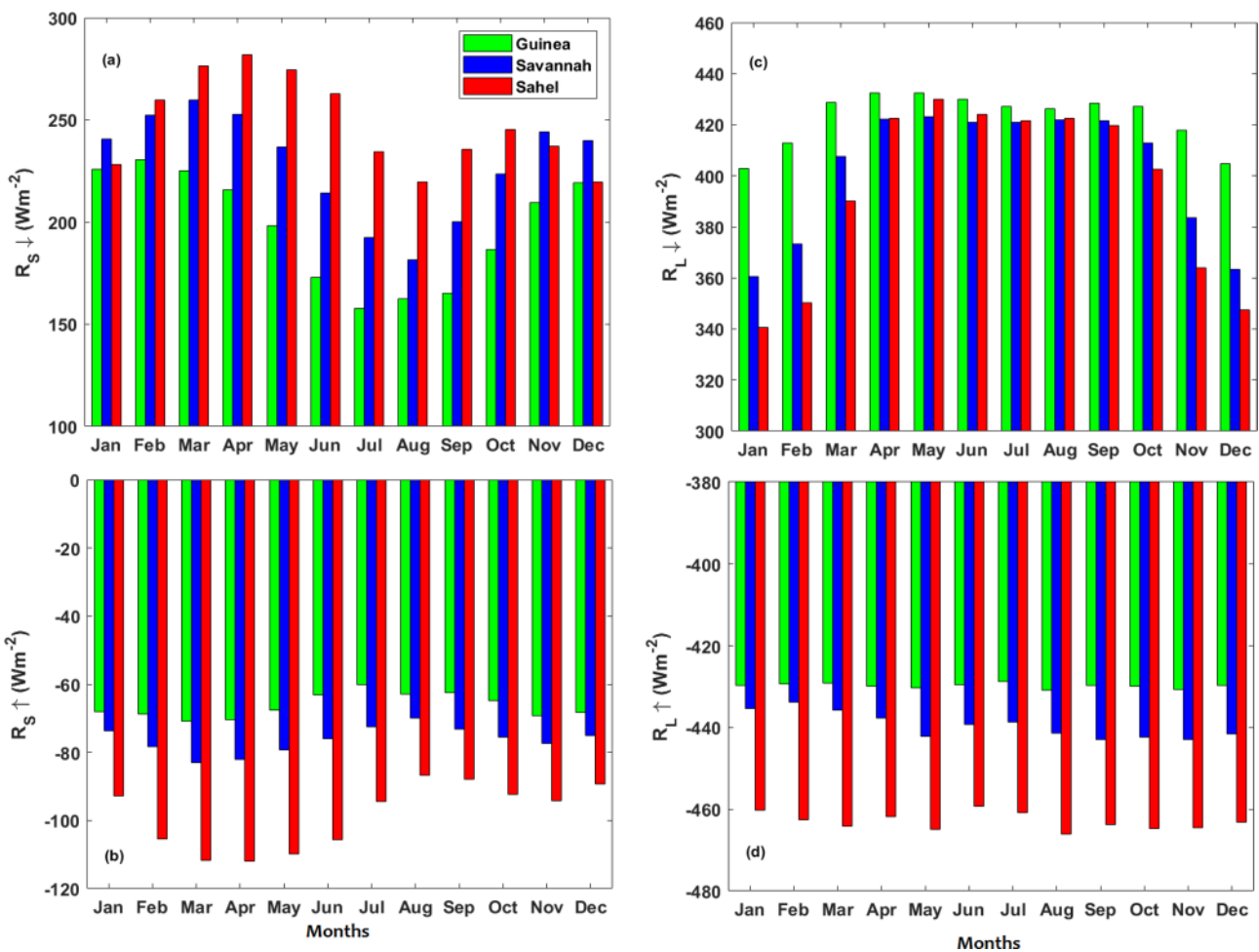


Fig. 7 Monthly mean variations in radiation components over Guinea, Savannah, and Sahel regions of Nigeria (1983–2018): **a** downwelling SW, $R_{S\downarrow}$, **b** upwelling SW, $R_{S\uparrow}$, **c** downwelling LW, $R_{L\downarrow}$ and

d upwelling LW radiations, $R_{L\uparrow}$. By convention, positive and negative signs denote downwelling and upwelling radiation components, respectively

over Guinea and Savannah zones but positive and insignificant ($r \leq 0.40$) over most parts of the Sahel (Fig. 9a). In addition, cloud cover showed positive and significant correlation ($r \sim 0.60$) with $R_{S\uparrow}$ over Guinea, while the positive correlations ($r \leq 0.40$) obtained over most parts of Savannah and Sahel were insignificant (Fig. 9b). The correlations between cloud cover and $R_{L\downarrow}$ were generally high, positive and significant ($0.90 \leq r \leq 0.99$) over the entire country (Fig. 9c). However, $R_{L\uparrow}$ produced negative and significant ($-0.90 \leq r \leq -0.99$) correlations with cloud cover over the entire country (Fig. 9d). These are indications that increased cloud cover fraction enhances $R_{L\downarrow}$ but inhibits $R_{L\uparrow}$. As expected, net all-wave radiation, R exhibited significant negative correlations ($-0.70 \leq r \leq -0.95$) with cloud cover over the entire country (Fig. 9e). The interpretation is that, future increase in cloudiness could lead to decrease in surface net radiation. However, r values obtained for cloud cover and temperature were generally negative over Guinea ($r \sim -0.45$) but positive over most

parts of Savannah and Sahel ($r \sim 0.65$); all significant at $p < 0.05$ (Fig. 9f). It suggests that the higher the cloud cover the more the surface cooling (i.e., lower temperature) over Guinea but more warming over the semi-arid regions. The result is a clear signal that cloudiness plays a major role in modulating surface radiation budget and temperature over the country.

3.5 Impacts of cloudiness on surface radiation budget and temperature

Table 2 gives the summary of regression analysis carried out to describe the contribution of cloudiness to surface radiation balance and temperature. The total variance explained by cloud cover (i.e., its contribution) to net all-wave radiation were found to be 23.9% (Guinea), 25.8% (Savannah) and 21.0% (Sahel); all significant at $p < 0.05$ (Table 2). In addition, cloud cover had significant impacts (20–33%) on all the four radiation components

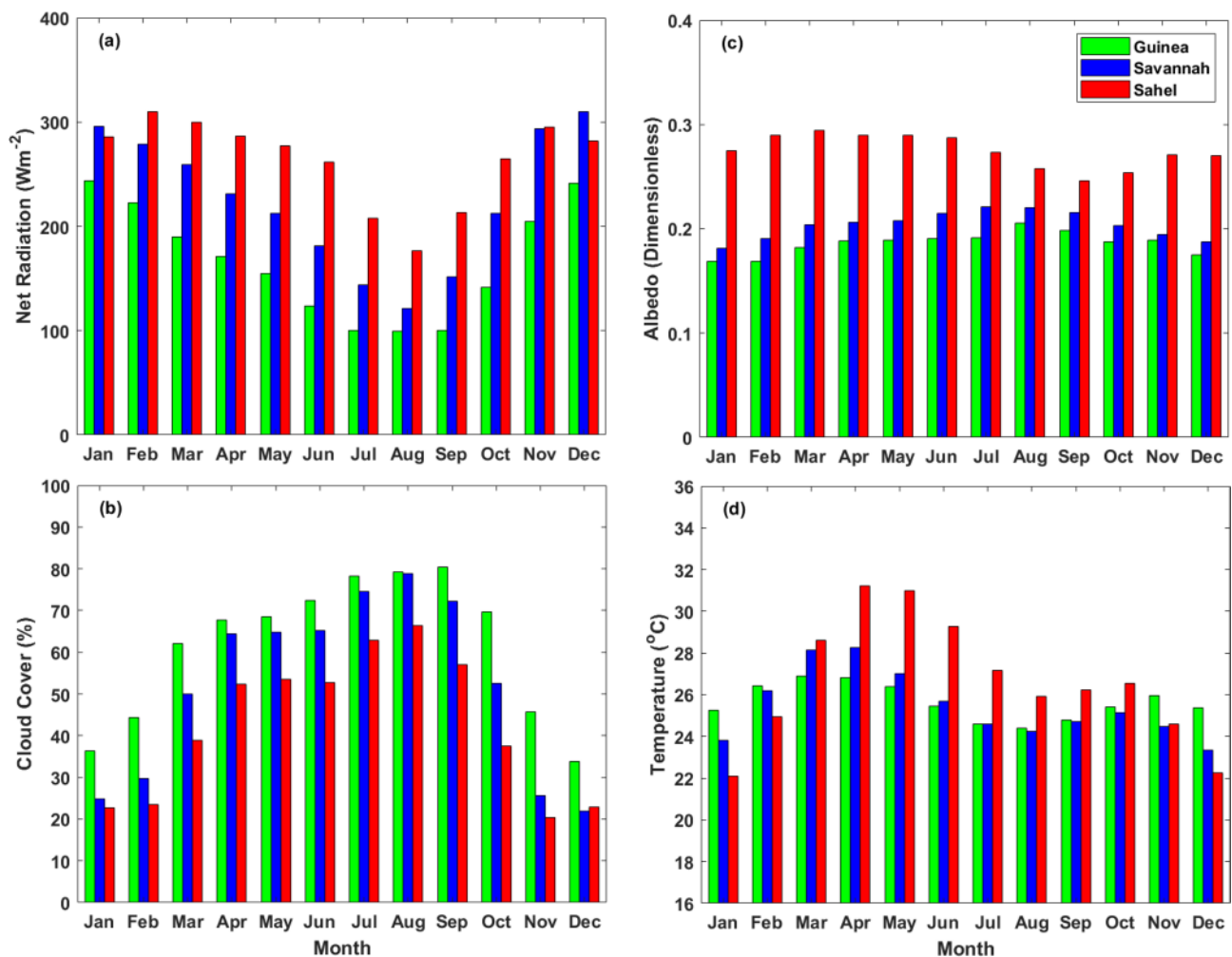


Fig. 8 Monthly mean variations (mean and standard deviation, STD) of **a** net radiation, **b** cloud cover fraction, **c** albedo, and **d** near surface temperature over Guinea, Savannah, and Sahel regions of Nigeria (1983–2018)

in the country except for both R_{S1} and R_{S_L} over Sahel and R_{S1} over Savannah. The total variance explained by cloud cover to variation in temperature were 2.3% (Guinea), 2.0% (Savannah) and 13.8% (Sahel). The changes in temperature accounted for by 13.8% variation in the predictor (cloud cover) over Sahel was found to be significant at $p < 0.05$. This suggested that cloud cover had insignificant impacts on temperature over Guinea and Savannah. This could be attributed to the influence of WAM and forest on warming reduction over the region as reported in previous studies [52, 84].

Figure 10 explains cloud-radiative effects (CRE) in R_S (tagged CRE_{SW}) and R_L (tagged CRE_{LW}) radiation over Nigeria. Negative CRE means cooling effects, while positive indicates warming. Generally, the estimated CRE_{SW} was negative (Fig. 10a), while CRE_{LW} was positive (Fig. 10b) over the entire country. It suggested cloud-radiative cooling effect of R_S which decreased latitudinally from the

coast to continental areas and heating effect of R_L which showed increment from the coast to the continental areas. For example, estimated CRE_{SW} were $-55 Wm^{-2}$ (Guinea), $-30 Wm^{-2}$ (Savannah) and $-10 Wm^{-2}$ (Sahel), while CRE_{LW} were 25, 45 and $65 Wm^{-2}$ in Guinea, Savannah and Sahel zones, respectively. The heating effect of CRE_{LW} in the northern parts of the country was completely neutralized by cooling effect of CRE_{SW} to produce a net surface warming (positive CRE) over the zones ($25 Wm^{-2}$ in Savannah and $50 Wm^{-2}$ in Sahel; Fig. 10c). Miller et al. [40] have also reported similar pattern of net cloud-radiative effects over the West African Sahel. The resultant heating effects of CRE in Sahel could be attributed to the enhanced R_{L1} due to higher surface temperature triggered by higher incoming solar radiation and overall drier and less cloudy atmosphere compared to Guinea zone [83]. However, heating effect of CRE_{LW} in the coastal areas was not strong enough to neutralize the cooling effect of CRE_{SW} and thus

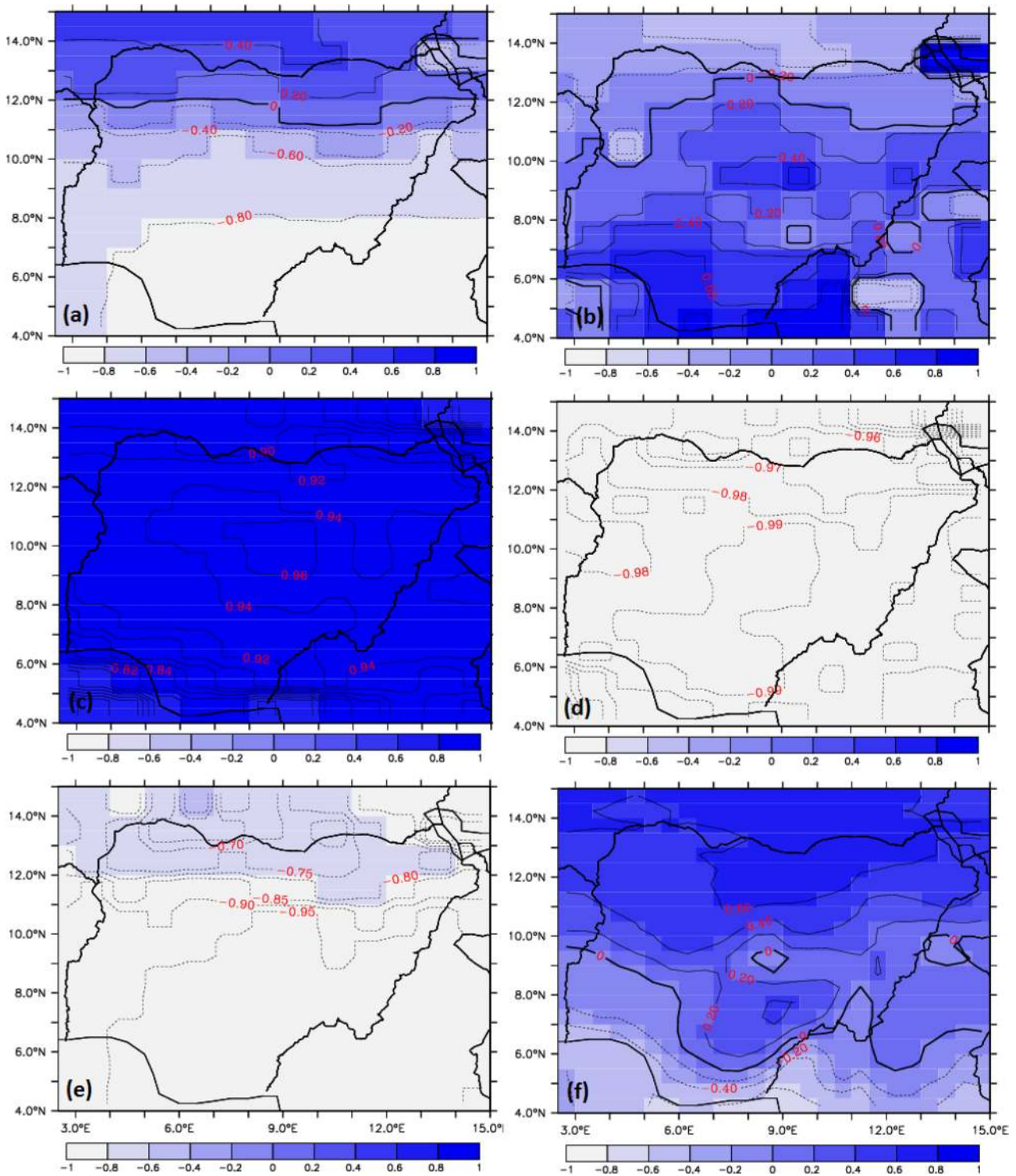


Fig. 9 Correlation coefficients, r between cloudiness and **a** downwelling SW, $R_{S\downarrow}$, **b** upwelling SW, $R_{S\uparrow}$, **c** downwelling LW, $R_{L\downarrow}$, **d** upwelling LW, $R_{L\uparrow}$, **e** net radiation, R , and **f** near surface temperature

a net cooling cloud-radiative effect was obtained over the region (-30 Wm^{-2} ; Fig. 10c). These patterns of results and the range of values obtained are in agreement with

those reported in Henderson et al. [26] and Wild et al. [87]. Finally, our findings demonstrated that the surface radiation budget and temperature over the country were

Table 2 Results of linear regression models of monthly time series of cloudiness (as an independent or explanatory variable), surface radiation components and temperature in different designated climatic regions of Nigeria

Zone	Regression parameter	Dependent variable					
		$R_{S\downarrow}$	$R_{S\uparrow}$	$R_{L\downarrow}$	$R_{L\uparrow}$	R	T
Guinea	Regression coefficient	-1.325*	0.135*	0.547*	-2.463*	-0.074*	-0.015
	Standard error	0.288	0.050	0.090	0.095	0.006	0.015
	95% Confidence Interval (lower, upper)	-1.343, -1.306	0.132, 0.139	0.541, 0.553	-2.470, -2.457	-0.075, -0.074	-0.016, -0.014
	Total variance explained	0.174	0.109	0.201	0.251	0.239	0.023
Savannah	Regression coefficient	-0.829*	0.039	1.117*	-3.214*	-0.069*	0.020
	Standard error	0.279	0.057	0.120	0.146	0.007	0.023
	95% Confidence Interval (upper, lower)	-0.847, -0.811	0.035, 0.043	1.109, 1.125	-3.223, -3.205	-0.070, -0.069	0.019, 0.022
	Total variance explained	0.135	0.013	0.258	0.281	0.258	0.020
Sahel	Regression coefficient	0.164	-0.016	1.898*	-3.962*	-0.046*	0.111*
	Standard error	0.412	0.179	0.233	0.266	0.011	0.043
	95% Confidence Interval (upper, lower)	0.138, 0.191	-0.028, -0.005	1.883, 1.913	-3.980, -3.945	-0.047, -0.045	0.108, 0.114
	Total variance explained	0.006	0.000	0.300	0.331	0.210	0.138

$R_{S\downarrow}$ = Downwelling shortwave radiation; $R_{S\uparrow}$ = Upwelling shortwave radiation

$R_{L\downarrow}$ = Downwelling longwave radiation; $R_{L\uparrow}$ = Upwelling longwave radiation

R = Net (all-wave) radiation; T = surface temperature

*Significant at $p < 0.05$

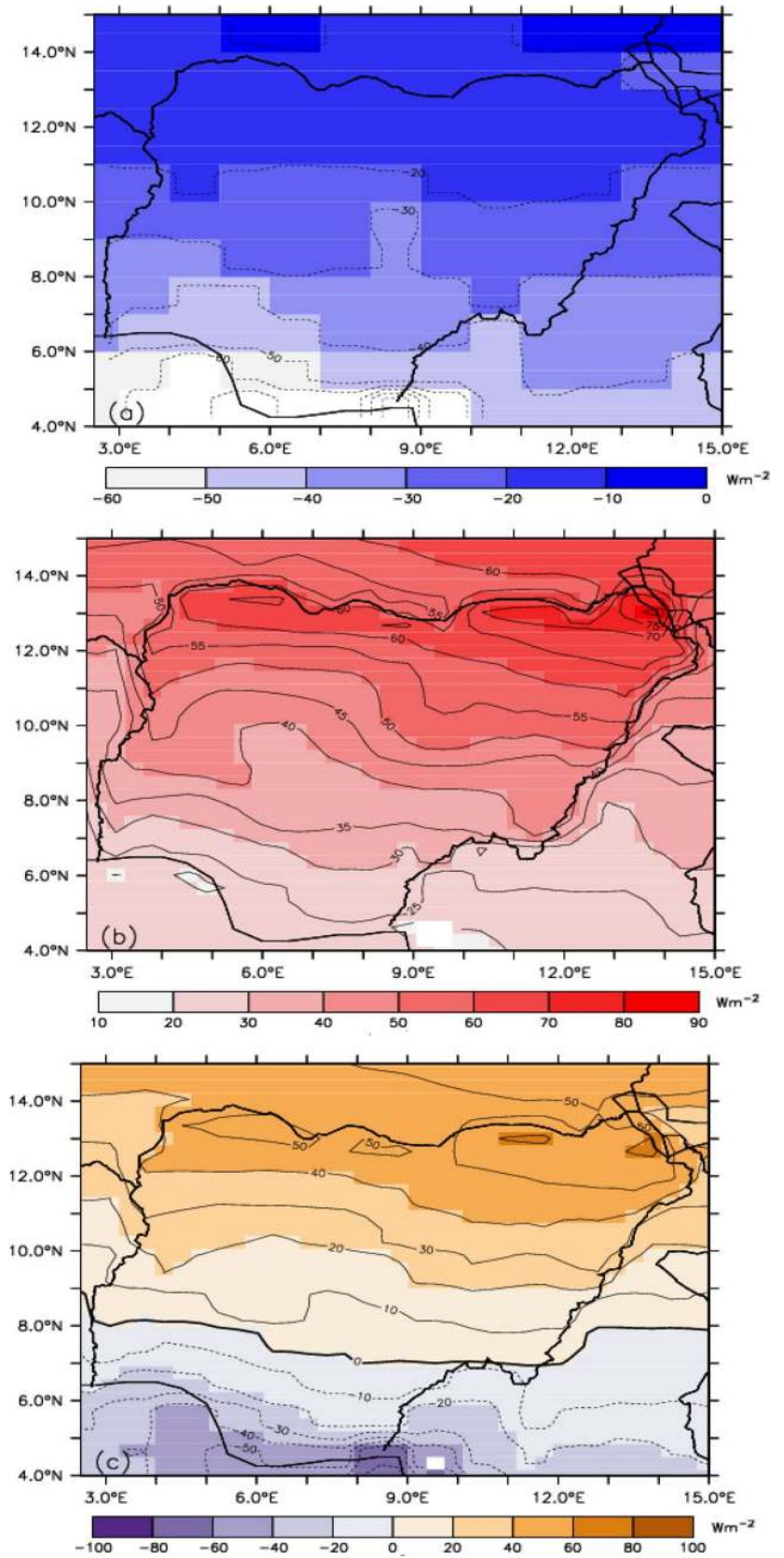
significantly impacted by changes in cloudiness due to cloud-radiative effects [36, 88, 89].

4 Conclusion

This study has investigated the impacts of cloudiness on near surface radiation and temperature in Nigeria, West Africa. To achieve this objective, it used the Modern-Era Retrospective Analysis for Research and Applications (MERRA) datasets sponsored by the National Aeronautics and Space Administration (NASA). Our findings revealed that:

1. Downwelling shortwave (SW) radiation ($R_{S\downarrow}$), upwelling longwave (LW) radiation ($R_{L\uparrow}$), net (all-wave) radiation and temperature increased latitudinally from the coast to inland or continental areas. However, cloud cover and downwelling LW radiations ($R_{L\downarrow}$) were found to decrease inland from the coast.
2. Inter-annual and seasonal changes in cloud cover, temperature and the radiation budget components varied significantly across the three designated climate zones (i.e., Guinea, Savannah and Sahel).
3. Under all-sky conditions, significant decreasing trends in $R_{S\downarrow}$ (-0.207 to $-0.268 \text{ Wm}^{-2} \text{ year}^{-1}$) and $R_{S\uparrow}$ (-0.165 to $-0.218 \text{ Wm}^{-2} \text{ year}^{-1}$) were obtained in most parts of the country. However, results indicated that there have been statistically significant increases in $R_{L\downarrow}$ (0.257 – $0.585 \text{ Wm}^{-2} \text{ year}^{-1}$) and $R_{L\uparrow}$ (0.124 – $0.422 \text{ Wm}^{-2} \text{ year}^{-1}$) during the study period. In addition, significant decreasing trends (-0.110 to $-0.536 \text{ Wm}^{-2} \text{ year}^{-1}$) in R but significant increasing trends in cloud cover were obtained in most parts of the country.
4. Under clear-sky conditions, however, all the four radiation components showed increasing trends (0.114 – $0.559 \text{ Wm}^{-2} \text{ year}^{-1}$) in most parts of the country while R indicated significant increasing R trends (0.256 – $0.807 \text{ Wm}^{-2} \text{ year}^{-1}$) in all zones.
5. The annual trends of temperature under all-sky (0.009 – $0.059 \text{ }^\circ\text{C year}^{-1}$) and clear-sky (0.019 – $0.072 \text{ }^\circ\text{C year}^{-1}$) conditions were observed to have increased significantly over the entire region.
6. The relationship between monthly average values of cloud cover and net radiation was negative and significant at $p < 0.05$ over the entire country. However, relationship between cloud cover and temperature was significant and negative over Guinea but positive over most parts of Savannah and Sahel.
7. Furthermore, changes in LW radiation components and net radiation were accounted for by 20 to 33%

Fig. 10 Cloud-radiative effects (CRE) in **a** SW, CRE_{SW} **b** LW, CRE_{LW} and **c** net CRE over Nigeria (1983–2018)



variations in cloud cover and the contributions were found to be significant across the zones.

8. Cloud-radiative cooling effect of SW radiation (CRE_{SW}) decreased latitudinally from the coast to inland areas, while the cloud-radiative heating effect of LW radiation (CRE_{LW}) increased inland from the coast. Furthermore, the heating effect of CRE_{LW} in the Savannah and Sahel zones was completely defused by cooling effect of CRE_{SW} to produce a net surface warming (25 Wm^{-2} (Savannah) and 50 Wm^{-2} (Sahel)). In the Guinea zone, however, a net cooling cloud-radiative effect (-30 Wm^{-2}) was obtained.
9. We concluded that the surface radiation budget and temperature were significantly impacted by variations in cloudiness over the country.
10. The study has implications for improved understanding of the role of clouds in moderating the surface radiation budget and temperature in different climatic zones of Nigeria, West Africa.
11. Presumably, the uncertainties in the NASA's MERRA reanalysis due to its relatively coarse resolution could limit the utility of the datasets for this research. Thus, further work is necessary to confirm the findings of this present study using high-resolution reanalyses and ground station observations of surface solar radiation components.

Acknowledgements The authors are indebted to the National Aeronautics and Space Administration (NASA) and the collaborating Institutions and Agencies under the Prediction of Worldwide Energy Resource (POWER) project for providing the climatological datasets used in this study.

Compliance with ethical standards

Conflict of interest The authors declare that they have no competing interests.

References

1. Zhao D, Aili A, Zhai Y, Xu S, Tan G, Yin X, Yang R (2019) Radiative sky cooling: fundamental principles, materials, and applications. *Appl Phys Rev* 6:021306. <https://doi.org/10.1063/1.5087281>
2. Delgado-Bonal A, Marshak A, Yang Y, Holdaway D (2020) Analyzing changes in the complexity of climate in the last four decades using MERRA-2 radiation data. *Sci Rep* 10:922. <https://doi.org/10.1038/s41598-020-57917-8>
3. Ramanathan V, Cess R, Harisson E, Minnis P, Barkstrom B, Ahmad A, Hartmann D (1989) Cloud-radiative forcing and climate: results from the earth radiation budget experiment. *Science* 243:57–63
4. Collow ABM, Miller MA (2016) The seasonal cycle of the radiation budget and cloud radiative effect in the Amazon rain forest of Brazil. *J Clim* 29:7703–7722. <https://doi.org/10.1175/JCLI-D-16-0089.1>

5. Stephens GL, O'Brien D, Webster PJ, Pilewski P, Kato S, Li JL (2015) The albedo of Earth. *Rev Geophys* 53:141–163
6. Zhou C, Zelinka MD, Klein SA (2016) Impact of decadal cloud variations on the Earth's energy budget. *Nat Geosci* 9:871–874. <https://doi.org/10.1038/ngeo2828>
7. Allen SJ, Wallance JS, Gash JHC, Savakumar MVK (1994) Measurement of albedo variation over natural vegetation. *Int J Climatol* 14:625–636
8. Stull RB (2012) An introduction to boundary layer meteorology, vol 13. Atmospheric and Oceanographic Sciences Library, Berlin
9. Ayoola MA, Sunmonu LA, Bashiru MI, Jegede OO (2014) Measurements of net all-wave radiation at a tropical location, Ile-Ife, Nigeria. *Atmósfera* 27(3):305–315
10. Hu YH, Jia GS, Pohl C, Zhang XX, van Genderen J (2016) Assessing surface albedo change and its induced radiation budget under rapid urbanization with Landsat and GLASS data. *Theor Appl Climatol* 123:711–722
11. Houspanossian J, Gimenez R, Jobbagy E, Noretto M (2017) Surface albedo raise in the South American Chaco: combined effects of deforestation and agricultural changes. *Agric For Meteorol* 232:118–127
12. Liang S, Wang D, He T, Yu Y (2019) Remote sensing of earth's energy budget: synthesis and review. *Int J Digit Earth* 12(7):737–780. <https://doi.org/10.1080/17538947.2019.1597189>
13. Ten-Berge HFM (1990) Heat and water transfer in bare top soil and the lower atmosphere. Simulation monographs, vol 33. Pudoc Wageningen, Wageningen, p 207
14. Pyrina M, Hatzianastassiou N, Matsoukas C, Fotiadi A, Papadimas CD, Pavlakis KG, Vardavas I (2013) Cloud effects on the solar and thermal radiation budgets of the Mediterranean basin. *Atmos Res*. <https://doi.org/10.1016/j.atmosres.2013.11.009>
15. Audu MO, Isikwue BC, Eweh JE (2014) Estimation of seasonal and annual albedo of the earth's atmosphere over Kano, Nigeria. *IOSR J Appl Phys* 5(6):56–62
16. He T, Liang S, Wang D, Shi Q, Tao X (2014) Estimation of high-resolution land surface shortwave albedo from AVIRIS data. *IEEE J Appl Earth Observ Remote Sens* 7:4919–4928
17. Chen X, Liang S, Cao Y, He T, Wang D (2015) Observed contrast changes in snow cover phenology in northern middle and high latitudes from 2001 to 2014. *Sci Rep* 5:16820
18. Chen D, Loboda TV, He T, Zhang Y, Liang S (2018) Strong cooling induced by stand-replacing fires through albedo in Siberian larch forests. *Sci Rep* 8:4821
19. Intergovernmental Panel on Climate Change (IPCC) (2001) Climate change 2001. In: Houghton JT et al (eds) The scientific basis. Cambridge University Press, New York, p 944
20. Kiehl JT, Trenberth KE (1997) Earth's annual global mean energy budget. *Bull Am Meteorol Soc* 78:197–208
21. Collins W, Ramaswamy V, Schwarzkopf MD, Sun Y, Portmann RW, Fu Q, Casanova SEB, Dufresne J-L et al (2006) Radiative forcing by well-mixed greenhouse gases: estimates from climate models in the intergovernmental panel on climate change (IPCC) fourth assessment report (AR4). *J Geophys Res* 111(D14):D14317
22. Soneye OO, Ayoola MA, Ajao IA, Jegede OO (2019) Diurnal and seasonal variations of the incoming solar radiation flux at a tropical station, Ile-Ife, Nigeria. *Heliyon* 5(5):e01673.7. <https://doi.org/10.1016/j.heliyon.2019.e01673>
23. Ceppi P, Briant F, Zelinka MD, Hartmann DL (2017) Cloud feedback mechanisms and their representation in global climate models. *WIREs Clim Change*. <https://doi.org/10.1002/wcc.465>
24. Stephens GL (2005) Cloud feedbacks in the climate system: a critical review. *J Clim* 18:237–273
25. Bouniol D, Couvreux F, Kamsu-Tamo P-H, Leplay M, Guichard F, Favot F (2012) Diurnal and seasonal cycles of cloud occurrences, types, and radiative impact over West Africa. *J Appl Meteorol Climatol* 51:534–553. <https://doi.org/10.1175/JAMC-D-11-051.1>

26. Henderson DS, L'Ecuyer T, Stephens G, Partain P, Sekiguchi M (2013) A multi-sensor perspective on the radiative impacts of clouds and aerosols. *J Appl Meteorol Climatol* 52:53–871. <https://doi.org/10.1175/jamc-d-12-025.1>
27. Yamasoe MA, do Rosário NME, Barros KM (2017) Downward solar global irradiance at the surface in São Paulo city—the climatological effects of aerosol and clouds. *J Geophys Res Atmos* 122:391–404. <https://doi.org/10.1002/2016JD025585>
28. Jia R, Luo M, Liu YZ, Zhu QZ, Hua S, Wu CQ, Shao TB (2019) Anthropogenic aerosol pollution over the eastern slope of the Tibetan Plateau. *Adv Atmos Sci* 36(8):847–862. <https://doi.org/10.1007/s00376-019-8212-0>
29. Soni VK, Pandithurai G, Pai DS (2012) Evaluation of long-term changes of solar radiation in India during clear day, cloudy day, foggy day and dust day. *Int J Climatol* 32:540–551
30. Hang Y (2016) The effect of cloud type on earth's energy balance. A thesis submitted in partial fulfilment of the requirements for the degree of Master of Science (Atmospheric and Oceanic Sciences) at the University of Wisconsin-Madison. p 137
31. Yeo H, Park S-J, Kim B-M, Shiobara M, Kim S-W, Kwon H, Kim J-H, Jeong J-H, Park SS, Choi T (2018) The observed relationship of cloud to surface longwave radiation and air temperature at Ny-Ålesund, Svalbard. *Tellus B Chem Phys Meteorol* 70:1450589. <https://doi.org/10.1080/16000889.2018.1450589>
32. Tzoumanikas P, Nikitidou E, Bais AF, Andreas Kazantzidis A (2016) The effect of clouds on surface solar irradiance, based on data from an all-sky imaging system. *Renew Energy* 95:314–322. <https://doi.org/10.1016/j.renene.2016.04.026>
33. Harrop BE, Hartmann DL (2016) The role of cloud radiative heating in determining the location of the ITCZ in Aquaplanet simulations. *J Clim* 29:2741–2763
34. Slingo A, Slingo JM (1988) The response of a general circulation model to cloud longwave radiative forcing. I: introduction and initial experiments. *Q J R Meteorol Soc* 114(482):1027–1062
35. Slingo JM, Slingo A (1991) The response of a general circulation model to cloud longwave radiative forcing. II: further studies. *Q J R Meteorol Soc* 117(498):333–364
36. Hill PG, Allan RP, Chiu JC, Bodas-Salcedo A, Knippertz P (2018) Quantifying the contribution of different cloud types to the radiation budget in Southern West Africa. *J Clim* 31:5273–5291. <https://doi.org/10.1175/JCLI-D-17-0586.1>
37. Jegede OO (1997) Daily averages of net radiation measured at Osu, Nigeria in 1995. *Int J Climatol* 17:1357–1367
38. Jegede OO (2002) Observations of daytime surface energy balance in cloudy tropical conditions at Ile-Ife, Nigeria. *MAUSAM* 53(3):359–366
39. Mallet M, Tulet P, Sercxa D, Solmon F, Dubovik G, Pelon J, Pont V, Thouron O (2009) Impact of dust aerosols on the radiative budget, surface heat fluxes, heating rate profiles and convective activity over West Africa during March 2006. *Atmos Chem Phys* 9:7143–7160
40. Miller MA, Ghate VP, Zahn RK (2012) The radiation budget of the West African Sahel and its controls: a perspective from observations and global climate models. *J Clim* 25:5976–5996. <https://doi.org/10.1175/JCLI-D-11-00072.1>
41. Collow ABM, Ghate VP, Miller MA, Trabachino L (2016) A one-year study of the diurnal cycle of meteorology, clouds, and radiation in the West African Sahel region. *Q J R Meteorol Soc* 142:16–29. <https://doi.org/10.1002/qj.2623>
42. Bonkaney A, Madougou S, Adamou R (2017) Impacts of cloud cover and dust on the performance of photovoltaic module in Niamey. *J Renew Energy*. <https://doi.org/10.1155/2017/9107502>
43. Li F, Vogelmann AM, Ramanathan V (2004) Saharan dust aerosol radiative forcing measured from space. *J Clim* 17:2558–2571
44. Sawadogo W, Abiodun BJ, Okogbue EC (2019) Impact of global warming on photovoltaic power generation over West Africa. *Renew Energy*. <https://doi.org/10.1016/j.renene.2019.11.032>
45. Nielsen LB, Berkowicz R, Conradsen K, Prahm LP (1981) Net incoming radiation estimated from hourly global radiation and/or cloud observations. *J Climatol* 1:255–272
46. Grist JP, Nicholson SE (2001) A study of the dynamic factors influencing the rainfall variability in the West African Sahel. *J Clim* 14:1337–1359
47. Afesimama EA, Pal JS, Abiodun BJ, Gutowski, Adedoyin A, WJ Jr., Adedoyin A (2006) Simulation of West African monsoon using the RegCM3. Part I: model validation and inter-annual variability. *Theor Appl Climatol* 86:23–37. <https://doi.org/10.1007/s00704-005-0202-8>
48. Gbode IE, Adeyeri OE, Menang KP, Intsiful JDK, Ajayi VO, Omotosho JA, Akinsanola AA (2019) Observed changes in climate extremes in Nigeria. *Meteorol Appl* 26:642–654. <https://doi.org/10.1002/met.1791>
49. Odekunle TO (2004) Rainfall and the length of the growing season in Nigeria. *Int J Climatol* 24:467–479. <https://doi.org/10.1002/joc.1012>
50. Odekunle TO (2010) An assessment of the influence of the Inter-Tropical Discontinuity on inter-annual rainfall characteristics in Nigeria. *Geograph Res* 48(3):314–326
51. Oguntunde PG, Abiodun BJ, Lischeid G (2011) Rainfall trends in Nigeria, 1901–2000. *J Hydrol* 411:207–218. <https://doi.org/10.1016/j.jhydrol.2011.09.037>
52. Abiodun BJ, Salami AT, Matthew OJ, Odedokun S (2012) Potential impacts of afforestation on climate change and extreme events in Nigeria. *Clim Dyn* 41:273–293. <https://doi.org/10.1007/s00382-012-1523-9>
53. Rienecker MM, Suarez MJ, Gelaro R, Todling R, Bacmeister J, Liu E, Bosilovich MG, Schubert SD, Takacs L et al (2011) MERRA: NASA's modern-era retrospective analysis for research and applications. *J Clim* 24:3624–3648
54. Westberg DJ, Stackhouse PW Jr, Crawley DB, Hoell JM, Chandler WS, Zhang T (2013) An analysis of NASA's MERRA meteorological data to supplement observational data for calculation of climatic design conditions. *ASHRAE Trans* 119(2):210–221
55. Ohunakin OS, Adaramola MS, Oyewola OM, Matthew OJ, Fagbenle RO (2015) The effect of climate change on solar radiation in Nigeria. *Sol Energy* 116:272–286. <https://doi.org/10.1016/j.solener.2015.03.027>
56. Osinowo AA, Okogbue EC, Ogungbenro SB, Fashanu O (2015) Analysis of global solar irradiance over climatic zones in Nigeria for solar energy applications. *Sol Energy*. <https://doi.org/10.1155/2015/819307>
57. Zhang X, Lu N, Jiang H, Yao L (2020) Evaluation of reanalysis surface incident solar radiation data in China. *Sci Rep* 10:3494. <https://doi.org/10.1038/s41598-020-60460-1>
58. Tahir Z-uR, Ali MJ, Ahmad SU, Asim M, Hayat N, Azhar M, Hussain A (2018) Evaluation of solar radiation from MERRA, MERRA-2, ERA-Interim and CFSR reanalysis datasets against surface observations for Multan, Pakistan. *EuroSun 2018/ISES Conference*. <https://doi.org/10.18086/eurosun2018.09.04>
59. Salazar G, Gueymard C, Galdino JB, Vilela OC, Fraidenaich N (2020) Solar irradiance time series derived from high-quality measurements, satellite-based models, and reanalyses at a near-equatorial site in Brazil. *Renew Sustain Energy Rev* 117:109478. <https://doi.org/10.1016/j.rser.2019.109478>
60. Boilley A, Wald L (2015) Comparison between meteorological re-analyses from ERA-Interim and MERRA and measurements of daily solar irradiation at surface. *Renew Energy* 75:135–143. <https://doi.org/10.1016/j.renene.2014.09.042>
61. McNally A, Arsenault K, Kumar S, Shukla S, Peterson P, Wang S, Funk C, Peters-Lidard CD, Verdin JP (2017) Data descriptor:

- a land data assimilation system for sub-Saharan Africa food and water security applications. *Sci Data* 4:170012. <https://doi.org/10.1038/sdata.2017.12>
62. Ojo OS, Adeyemi B, Ogolo EO (2019) Assessment of the nighttime and daytime radiative fluxes balance on seasonal timescale over West Africa. *J Atmos Sol Terres Phys* 191:105048. <https://doi.org/10.1016/j.jastp.2019.05.012>
 63. Staley DO, Jurica GM (1972) Effective atmosphere emissivity under clear skies. *J Appl Meteorol* 11:349–356
 64. Mihailovic DT, Kallos G (1997) A sensitivity study of a coupled soil-vegetation boundary-layer scheme for use in atmospheric modeling. *Bound Layer Meteorol* 82:283–315
 65. Carmona F, Rivas R, Caselles V (2014) Estimation of daytime downward longwave radiation under clear and cloudy skies conditions over a sub-humid region. *Theor Appl Climatol* 115:281–295. <https://doi.org/10.1007/s00704-013-0891-3>
 66. Al-Lami A, Al-Salihi AM, Al-Timimi YK (2017) Parameterization of the downward longwave radiation under clear-sky conditions in Baghdad, Iraq. *Asian J Appl Sci* 10:10–17
 67. Fashae OA, Adagbasa EG, Olusola AO, Obateru RO (2020) Land use/land cover change and land surface temperature of Ibadan and environs, Nigeria. *Environ Monit Assess* 192:109. <https://doi.org/10.1007/s10661-019-8054-3>
 68. Van de Griend AA, Owe M (1993) On the relationship between thermal emissivity and the normalised difference vegetation index for natural surface. *Int J Remote Sens* 14:1119–1131
 69. Setturu B, Rajan KS, Ramachandra TV (2013) Land surface temperature responses to land use land cover dynamics. *Geoinform Geostat* 1:4. <https://doi.org/10.4172/2327-4581.1000112>
 70. Allen RG, Pereira LS, Raes D, Smith M (1998) Crop evapotranspiration—guidelines for computing crop water requirements. Food and Agriculture Organization UN, Rome
 71. Silva JB, Gaio DC, Curado LFA, Jde-S Nogueira, Valle LCG Jr., Rodrigues TR (2019) Evaluation of methods for estimating atmospheric emissivity in Mato-Grossense Cerrado. *Revista Ambiente & Água*. <https://doi.org/10.4136/ambi-agua.2288>
 72. Mann HB (1945) Non-parametric tests against trend. *Econometrica* 13:245–259
 73. Kendall MG (1975) Rank correlation methods, 4th edn. Charles Griffin, London, p 202
 74. Salmi T, Maatta A, Anttila P, Ruoho-Airola T, Amnell T (2002) Detecting trends of annual values of atmospheric pollutants by the Mann-Kendall Test and Sen's slope estimates. *Publications on Air Quality*, No. 31. Helsinki, Finland
 75. Tosic I, Unkasevic M (2005) Analysis of precipitation series for Belgrade. *Theor Appl Climatol* 80(1):67–77
 76. Alados I, Foyo-Moreno I, Olmo FJ, Alados-Arboleda L (2003) Relationship between net radiation and solar radiation for semi-arid shrub-land. *Agric For Meteorol* 116:221–227
 77. Smith GL, Rutan DA (2003) The diurnal cycle of outgoing longwave radiation from earth radiation budget experiment measurements. *J Atmos Sci* 60:1529–1542
 78. Kumar S, Srivastava AK, Pathak V, Bisht DS, Tiwari S (2019) Surface solar radiation and its association with aerosol characteristics at an urban station in the Indo-Gangetic Basin: implication to radiative effect. *J Atmos Sol Terr Phys* 193:105061. <https://doi.org/10.1016/j.jastp.2019.105061>
 79. Ojo O (1977) The climates of West Africa. Heinemann, London, p 219
 80. Hayward DF, Oguntoyinbo JS (1987) The climatology of West Africa. Rowan & Littlefield, New York, p 271
 81. Matzinger N, Andretta M, van Gorsel E, Vogt R, Ohmura A, Rotach MW (2003) Surface radiation budget in an Alpine valley. *Q J R Meteor Soc* 129:877–895
 82. Augustine JA, Dutton EG (2013) Variability of the surface radiation budget over the United States from 1996 through 2011 from high-quality measurements. *J Geophys Res Atmos* 118:43–53
 83. Kniffka A, Knippertz P, Fink AH (2019) The role of low-level clouds in the West African monsoon system. *Atmos Chem Phys* 19:1623–1647. <https://doi.org/10.5194/acp-19-1623-2019>
 84. Matthew OJ, Ohunakin OS (2017) Simulating the effects of climate change and afforestation on wind power potential in Nigeria. *Sustain Energy Technol Assess* 22:41–54. <https://doi.org/10.1016/j.seta.2017.05.009>
 85. Kothe S, Ahrens B (2010) On the radiation budget in regional climate simulations for West Africa. *J Geophys Res Atmos* 115:1984–2012
 86. Stull RB (1988) An introduction to boundary layer meteorology. Kluwer Academic Publishers, Dordrecht, p 666
 87. Wild M, Hakuba MZ, Folini D, Dörig-Ott P, Schär C, Kato S, Long CN (2018) The cloud-free global energy balance and inferred cloud radiative effects: an assessment based on direct observations and climate models. *Clim Dyn* 52:4787–4812. <https://doi.org/10.1007/s00382-018-4413-y>
 88. Myers TA, Norris JR (2015) On the relationships between subtropical clouds and meteorology in observations and CMIP3 and CMIP5 models. *J Clim* 28:2945–2967. <https://doi.org/10.1175/JCLI-D-14-00475.1>
 89. Hill PG, Allan RP, Chiu JC, Stein THM (2016) A multi-satellite climatology of clouds, radiation and precipitation in southern West Africa and comparison to climate models. *J Geophys Res Atmos* 121(10):857–879. <https://doi.org/10.1002/2016JD025246>

Publisher's Note Springer Nature remains neutral with regard to jurisdictional claims in published maps and institutional affiliations.